Semiconductor physics

Structure, optical, and photocatalytic properties of Cd-doped ZnO microstructures prepared by MOCVD at atmospheric pressure

V.A. Karpyna[1], **A.Y. Lemish**[1,2*], **L.A. Myroniuk**[1], **D.V. Myroniuk**[1], **O.I. Olifan**[1], **I.M. Danylenko**[3], **V.V. Bilorusets**[4], **S.P. Starik**[4], **V.V. Strelchuk**[3], **A.I. Ievtushenko**[1]

[1]*Frantsevich Institute for Problems of Materials Science, NAS of Ukraine, Kyiv, Ukraine*
[2]*National Technical University of Ukraine "Igor Sikorsky Kyiv Polytechnic Institute", Kyiv, Ukraine*
[3]*V. Lashkaryov Institute of Semiconductor Physics, NAS of Ukraine, Kyiv, Ukraine*
[4]*V. Bakul Institute for Superhard Materials, NAS of Ukraine, Kyiv, Ukraine*
[*]*Corresponding author e-mail: a.lemish-me24@lll.kpi.ua*

Abstract. This work aims to investigate the effect of cadmium dopant concentration on the properties of zinc oxide microstructures grown on silicon substrates by using metalorganic chemical vapor deposition at atmospheric pressure. The XRD patterns confirm the formation of a wurtzite-type crystalline phase of zinc oxide. The photoluminescence spectra of the studied ZnO microstructures consist of several bands, including a violet band (3.24 eV), blue band (2.8 eV), and yellow band (2.1 eV). The blue band was observed only for Cd-doped ZnO microstructures and was absent for undoped ZnO microstructures. ZnO microstructures grown with 1, 2.5, and 10 wt.% of Cd in the precursor mixture exhibited the best photocatalytic efficiency (over 70% degradation of Methyl Orange dye within 180 min). The higher reaction rate constant was observed for Cd-doped ZnO microstructures, for which the contribution of the blue band in the whole photoluminescence spectrum lies within the range 30…40% and the contribution of the violet band is close to 20%. The results obtained demonstrate that Cd-doped ZnO microstructures exhibit attractive photocatalytic activity and can be used for the development of effective photocatalysts.

Keywords: zinc oxide, cadmium, microstructures, MOCVD, photocatalysis, photoluminescence.

https://doi.org/10.15407/spqeo28.04.413
PACS 68.55.Ln, 77.55.hf, 78.55.Et, 81.15.Gh

Manuscript received 29.04.25; revised version received 14.10.25; accepted for publication 26.11.25; published online 15.12.25.

1. Introduction

Zinc oxide (ZnO) is a polar inorganic crystalline material, a direct-bandgap semiconductor with a wide energy band gap close to 3.3 eV at room temperature and a large exciton binding energy of 60 meV [1]. It is widely used as an additive in different materials and products. The unique combination of electrical and optical properties makes ZnO prospective for the semiconductor industry in the field of electronics, optoelectronics, and photovoltaics, especially for solar cells' design, ultraviolet light-emitting diodes, and photodetectors [2–4]. The physical properties of ZnO can be easily modified by appropriate doping, which opens a new horizon for a variety of applications in the semiconductor industry. For example, doping with In, Al, or Ga is often used to obtain high conductivity and optical transparency thin films [5, 6]. Zinc oxide is also an attractive material for photocatalytic applications [7]. However, the main disadvantage of zinc oxide as a photocatalyst is that its light absorption is only efficient within the UV part of the optical spectrum, which significantly limits its use for visible photocatalysis. To overcome this challenge and enhance the photocatalytic activity of ZnO doping with various metal and non-metal impurities, including rare-earth elements, has been proposed and investigated over the last 20 years. A significant number of studies have been devoted to the investigation of structure, morphology, and doping level impact on ZnO photocatalytic properties by using X-ray diffraction analysis, scanning electron microscopy, Raman scattering, and UV-vis spectroscopy. Three model organic solutions, namely Methyl Orange dye, Methylene Blue, or Rhodamine B dye, are often chosen to study the kinetics of the degradation process [8].

Among the number of doping elements, Cd is considered the most promising impurity for the reduction of the ZnO band gap [9, 10]. Bandgap engineering is desirable to achieve a bandgap that corresponds to the visible range of the optical spectrum [11, 12]. Cd has 2 valence electrons, like Zn. Thus, it does not create new donor or acceptor levels in the forbidden band. However, a significant difference in the ion radii of Zn^{2+} and Cd^{2+} results in a substantial change in the electronic structure of ZnO. The bandgap of $Zn_{1-x}Cd_xO$ solid solution can be varied within 3.3…2.2 eV, which allows tuning its properties within a wide optical wavelength range [13, 14]. Cd also effectively reduces the damage in ZnO caused by electrons [15] and heavy ions irradiation [16, 17].

For ZnO synthesis, a lot of chemical and physical methods are available. We can underline the sol-gel [18], spray pyrolysis [19, 20], chemical vapor deposition [21], hydrothermal synthesis and electrochemical deposition [22, 23], pulsed laser deposition, and magnetron sputtering [24]. All these methods are well studied and provide the synthesis of thin films with high reproducibility.

In this study, we try to use MOCVD at atmospheric pressure (APMOCVD) to grow Cd-doped ZnO microstructures. Among other things, it is worth noting that Cd and Zn have sufficient differences in saturation vapor pressure, which could result in extremely low incorporation of Cd ions into the growing ZnO phase. No results of ZnO:Cd synthesis by using the APMOCVD method exist. Possibly, this approach leads to new features of ZnO:Cd growth with distinct properties. Previously, properties of Cd-doped ZnO films grown using MOCVD with conventional diethyl-zinc and dimethyl-cadmium precursors were investigated in Refs. [25, 26]. Thus, this work is focused on studying the feasibility of using Zn and Cd acetylacetonates for the growth of Cd-doped ZnO microstructures and investigating the impact of various Cd acetylacetonate concentrations on the structure and properties of grown samples.

2. Experimental methods

2.1. Sample preparation

Zinc acetylacetonate $Zn(C_5H_7O_2)_2$ (99%) from J&K Scientific LTD and cadmium acetylacetonate $Cd(C_5H_7O_2)_2$ (>99.9%) from Tokyo Chemical Industry Co., LTD were used as precursors for the growth of undoped ZnO and Cd-doped ZnO microstructures by APMOCVD. The metal atom in the metalorganic compounds is characterized by weak bonds, and therefore, the compounds are easily decomposed at relatively low temperatures. The melting temperatures of zinc and cadmium acetylacetonates are 124…126 °C and 209…214 °C, respectively. Thus, the decomposition of these metalorganic compounds free the metal ions, which, in turn, is easily oxidized to the corresponding oxides. Hence, cadmium-doped zinc oxide can be obtained from a mixture of acetylacetonates of various metals in the appropriate ratio.

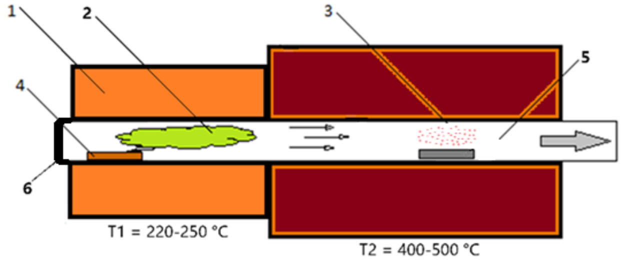

Fig. 1. Schematic view of the furnace for growing nanostructures using APMOCVD: *1* – precursor evaporation zone, *2* – precursor decomposition and transport zone, *3* – deposition zone, *4* – porcelain container (crucible) with precursors, *5* – quartz tube, *6* – ceramic plug.

The growth of ZnO microstructures on silicon substrates was carried out using the APMOCVD process in a tubular electric furnace with a length of 700 cm, a diameter of 5 cm, and a power of 2.5 kW. A schematic view of the furnace for growing nanostructures using APMOCVD is shown in Fig. 1. The furnace consists of three zones: zone *1* – for evaporation of precursors, zone *2* – chemical vapor transport zone, zone *3* – zone of condensation and growth of ZnO nanostructures.

The porcelain crucible with a mixture of zinc acetylacetonate (Zn(AA)) and cadmium acetylacetonate Cd(AA) precursors was placed in zone *1* of the furnace for decomposition. One end of the quartz tube was closed by a bung, and the other end of the tube was open to remove the reaction products. The substrates were placed in zone *3* of the furnace at a temperature of 400 to 500 °C. Naturally, the silicon substrates were cleaned in ethanol and deionized water using an ultrasonic bath. The cleaning lasted 360 s for each solvent, after which the wafers were dried in a nitrogen stream. After that, the substrates were placed in deposition zone *3* of the preheated furnace for heating to a temperature higher than 400…500 °C. Then, the porcelain crucible with a mixture of Zn(AA) and Cd(AA) precursors was placed in zone *1*, and the quartz tube was closed with a ceramic plug. The distance between the precursors and the silicon substrates was 7 cm. The deposition was carried out for 30 min, after which the furnace was turned off. The samples were cooled in the furnace for an hour.

2.2. Photocatalytic experiment

Photocatalytic activity of ZnO and Cd-doped ZnO photocatalysts was characterized using the model pollutant – methyl orange (MO) aqueous solution with optimal initial concentration 10 $mg \cdot L^{-1}$ [27] under Hg lamp irradiation with a power of 200 W. Methyl Orange dye is very stable, does not degrade at visible or UV light unless facilitated by a suitable photocatalyst. The distance from the irradiation source to the container with samples was at least 15 cm. Before illumination, the samples were washed with an MO solution to remove particles that did not adhere well to the silicon surface and could distort the results of the MO solution transmission. Then, samples of undoped and Cd-doped

ZnO deposited by MOCVD with an area close to 1×1 cm^2 were immersed in 3 ml of an aqueous solution of MO. The container with the samples was kept for 12 hours to obtain the adsorption equilibrium before irradiation. The samples were exposed to irradiation for 60, 120, and 180 min, respectively. The concentrations of MO dye were determined by measuring the transmittance of the MO solution at 465 nm at each stage of photo-degradation. This study was repeated several times on the same samples to confirm the validity of the photocatalyst reaction.

The degradation efficiency (DE) of MO was calculated using equation (1):

$$\text{Degradation efficiency (\%)} = (C_0 - C_t)/C_0\times100\%, \qquad (1)$$

where C_0 is the initial concentration of the MO dye and C_t is the concentration of the MO dye after irradiation for time t. The error of dye concentration measurement was no more than 0.1%.

The rate of the photodegradation reactions was described using the pseudo-first-order kinetic model:

$$\ln\left(C_0/C_t\right) = kt, \qquad (2)$$

where k is the pseudo-first-order rate constant [28].

2.3. Characterization

The structure of the ZnO:Cd was studied using an X-ray diffractometer DRON-4 under the simultaneous rotation of the sample and the counter (2θ curves). The 40 kV and 30 mA X-ray tube generated Cu$K_{\alpha1}$ radiation with a wave-length of $\lambda = 0.154056$ nm. The resolution was 0.01°.

Elemental analysis was carried out using two scanning electron microscopes: TESCAN MIRA 3 LMU and ZEISS EVO 50XVP. The samples were examined for the presence of Zn, O, and Cd as well as various potential impurities.

Raman spectra were recorded using the Horiba Jobin-Yvon T64000 spectrometer equipped with a CCD detector at room temperature in a backscattering geometry. Radiation from a solid-state laser (532 nm) and a He-Cd laser (325 nm) was focused on the sample by using an Olympus BX 41 microscope and used to study Raman scattering under non-resonant conditions. The diameter of the analyzed spot was 1 μm, and the spectral resolution was 1 cm^{-1} and 1 nm, respectively.

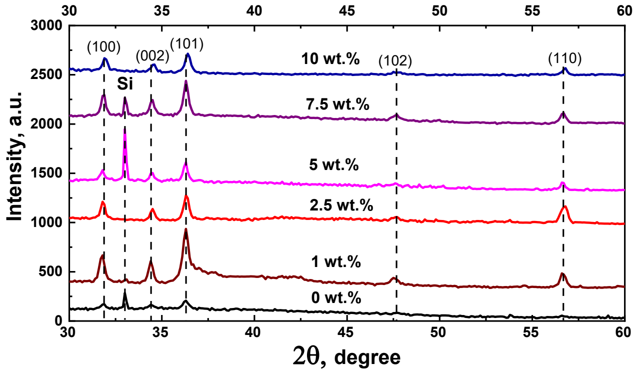

Fig. 2. X-ray diffraction pattern of ZnO/Si microstructures grown at various (0…10 wt.%) Cd(AA) precursor content.

The optical and photocatalytic properties were characterized by UV-VIS spectrometry by using a Shimadzu UV2600i dual-beam spectrophotometer.

3. Results and discussion

3.1. X-ray diffraction analysis

Fig. 2 shows X-ray diffraction patterns of undoped and Cd-doped ZnO microstructures. The XRD patterns confirm the formation of a wurtzite-type crystalline phase of zinc oxide. Intense reflexes are observed from (100), (002), (101), (110), and (110) planes. The peak related to Si is also observed. No additional phases associated with Cd (according to JCPDS cards No. 05-0674, No. 01-1176) or CdO (according to JCPDS cards No. 05-0640, No. 76-0653) were observed. Since the Cd^{2+} ion has a larger ionic radius than the Zn^{2+} ion (78 pm over 60 pm), the substitution of native Zn atoms by Cd atoms in the ZnO lattice can lead to an increase in the lattice period c. It is worth noting that ZnO has a wurtzite structure, while CdO has a rock salt structure, making it difficult to grow a wurtzite $Zn_{1-x}Cd_xO$ system with high Cd content. For x within 0…0.6, the c-axis length $c(x)$ as a function of Cd content can be expressed by the following equation: $c(x) = 0.5207 + 0.056x - 0.0029x^2$ [29]. In our case, the lattice constant c lies within 0.519…0.521 nm and demonstrates a slight decrease with increasing Cd. This means that only a small amount of Cd is incorporated into the ZnO lattice. The decrease in lattice constant c can be explained by increasing microstrain in the ZnO lattice (see Table 1).

Table 1. XRD data and lattice parameters for ZnO microstructures grown at various Cd(AA) precursor contents.

Cd(AA) concentration, wt.%	Diffraction angle 2θ, degree	FWHM, degree	Lattice constant c, nm	Grain size D, nm	Lattice strain ε_c
0	34.43	0.31	0.5203	27	$-5.76\cdot10^{-4}$
1	34.40	0.30	0.5207	28	$1.92\cdot10^{-4}$
2.5	34.50	0.28	0.5194	30	$-2.31\cdot10^{-3}$
5	34.46	0.26	0.5198	32	$-1.54\cdot10^{-3}$
7.5	34.47	0.27	0.5197	31	$-1.73\cdot10^{-3}$
10	34.54	0.28	0.5187	29	$-3.65\cdot10^{-3}$

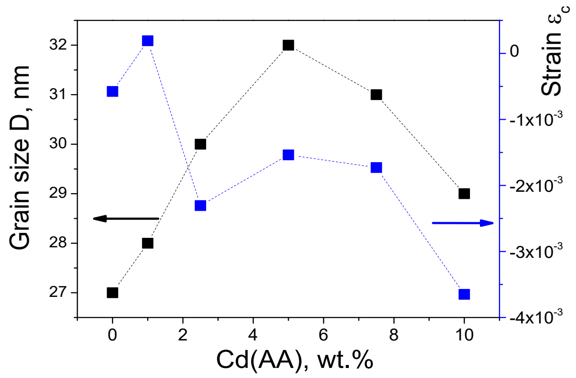

Fig. 3. Relationship between grain size D and lattice strain ε_c as a function of Cd(AA) concentration.

The microstrain along the c-axis was estimated using the following formula:

$$\varepsilon_c = \frac{c - c_0}{c_0}, \tag{3}$$

where $c_0 = 0.5206$ nm.

Grain size can be estimated by the Scherrer formula using the FWHM values of diffraction peaks of XRD patterns [30, 31]:

$$D = \frac{0.9\lambda}{FWHM \cdot \cos\theta}, \tag{4}$$

where D is the grain size, λ equals X-ray radiation wavelength, *FWHM* is the full width at half maximum of diffraction peak, and θ is the Bragg angle.

The calculated grain size D and microstrain ε_c in ZnO are shown in Fig. 3 as a function of Cd concentration in the mixture of the precursors. At first, the grain size D increases with Cd content up to 32 nm at 5 to 7.5 wt.% Cd and then slightly decreases to 29 nm. The microstrains, which are minimal in ZnO without Cd impurity, demonstrate compression of the c-axis by 0.36 %.

Scanning electron microscopy

The surface morphology of undoped and Cd-doped ZnO microstructures was investigated using scanning electron microscopy, and the results are shown in Figs 4a–4f.

One can see that the surface of the silicon wafers is uniformly covered with microstructures in the form of branched agglomerations due to chemical vapor deposition of metalorganic compounds (Zn and Cd acetylacetonates). Upon detailed inspection (inserts in the images), it is noticeable that these are highly agglomerated spherical particles with a size close to 1 μm. It should be noted that the ZnO microcrystals' agglomerations are oriented randomly without a preferred growth direction. In addition, doping with various Cd concentrations does not significantly affect the microcrystal size.

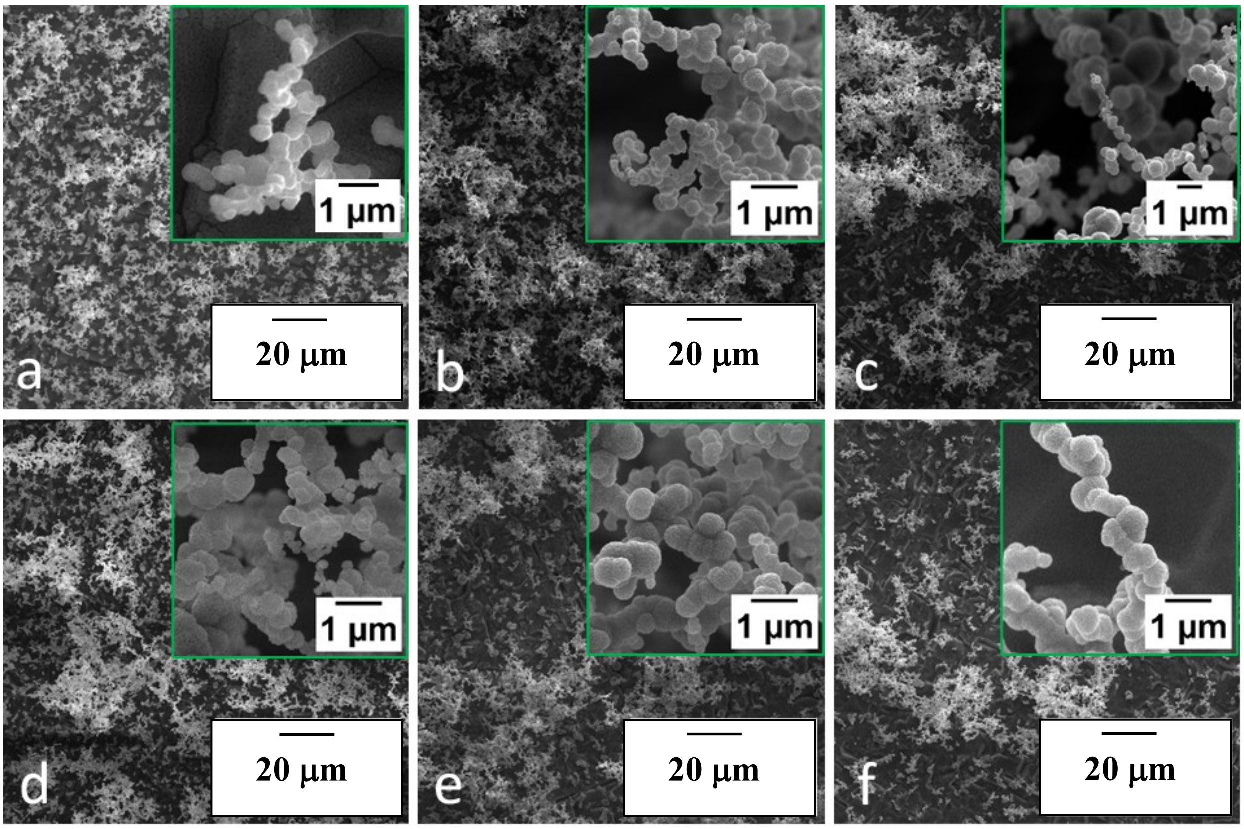

Fig. 4. Scanning electron microscopy images of ZnO deposited with various Cd(AA) concentrations, wt.%: 0 (*a*), 1 (*b*), 2.5 (*c*), 5 (*d*), 7.5 (*e*), 10 (*f*).

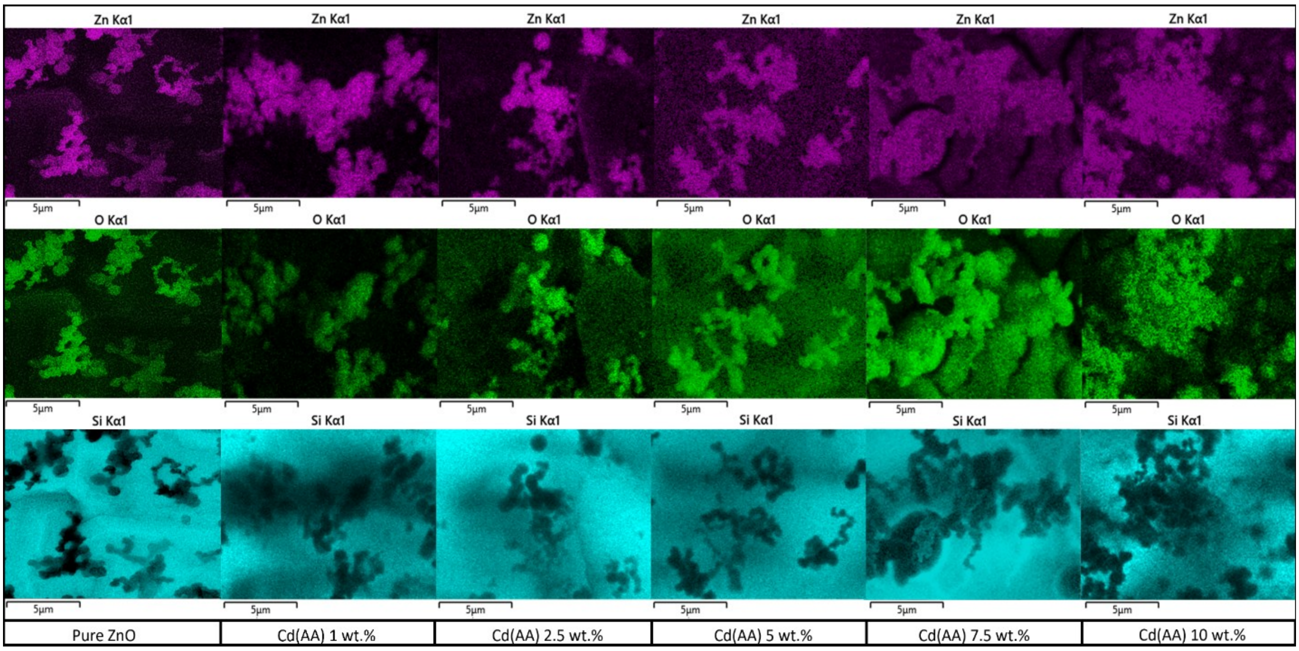

Fig. 5. Elemental distribution of pure and Cd-doped ZnO microcrystals (1, 2.5, 5, 7.5, and 10 wt.%).

EDX mapping was performed to investigate the elemental distribution in pure and ZnO:Cd microstructures. The elemental mapping image in Fig. 5 shows the distribution of Zn (purple), O (green), and Si (light blue) elements in ZnO microstructures doped with 1, 2.5, 5, 7.5, and 10 wt.% of Cd(AA), respectively.

The attentive eye can see that the images look brighter or darker, exhibiting an increase or decrease in Zn and O content. It should be noted that Cd content was not detected in the EDX analysis. Hence, one can suppose that Cd concentration is no more than 0.2 at.%, *i.e.*, lies below the minimal detection level of the EDX analyzer. However, the traces of carbon were present in each sample, probably due to carbon precipitation during the synthesis process, accompanied by Zn and Cd acetylacetonate decomposition. The measured values of Zn and O content are presented in Table 2.

The obtained microstructures are characterized by non-stoichiometry due to the lack of oxygen in the crystal lattice. This composition is typical for all oxides obtained using the MOCVD method. The big values of atomic percent of Si testify that ZnO microstructures do not fully cover the Si wafer. In this case, we cannot precisely measure the Zn/O ratio.

Table 2. Elemental distribution in ZnO microcrystal samples.

Cd(AA) concentration, wt.%	Zn, at.%	O, at.%	Si, at.%
0	36.7	36.2	27.2
1	44.1	35.3	20.6
2.5	37.7	32.6	29.8
5	28.4	23.9	47.7
7.5	49.5	36.8	13.7
10	40.7	38.5	20.8

3.2. Raman spectra

Raman spectra of initial ZnO and ZnO:Cd microstructures are shown in Fig. 6. Two peaks at close to 99 and 435.5 cm^{-1} are observed for all samples of ZnO:Cd microstructures, which are associated with vibrations of heavy zinc (cadmium) ions of the cationic sublattice E_2^{low} and light oxygen ions of the anionic sublattice E_2^{high}. The appearance of the E_2^{high} mode at 435.5 cm^{-1} is typical for the wurtzite hexagonal phase of ZnO and assigned to the optical phonon E_2 mode of ZnO crystal [32]. The weak mode at 330 cm^{-1} is associated with the $E_2^{high} - E_2^{low}$ band of the second order of ZnO. The A_1^{TO} mode at 383 cm^{-1} indicates the growth of ZnO crystallites with random orientation. The peak at 577 cm^{-1} is associated with the A_1^{LO} mode of ZnO, which is typically observed within 570…580 cm^{-1}. The slight shift can indicate lattice distortion due to the presence of Cd^{2+} ions with a bigger radius than Zn^{2+}.

The substitution of zinc ions by heavier cadmium ions causes a slight shift of the E_2^{low} mode towards a smaller frequency for samples with 1 and 2.5 wt.% of Cd(AA) compared to the undoped ZnO sample. However, for concentrations of 5, 7.5, and 10 wt.% of Cd(AA), the peak position of that mode goes back to the initial frequency (Fig. 7). Minor Cd doping facilitates defect generation and causes an increase in the amplitude of E_2^{low}. It is worth noting that the shift of the E_2^{low} mode is within the margin of error. Thus, the displacement of Zn^{2+} ions in the lattice is minimal.

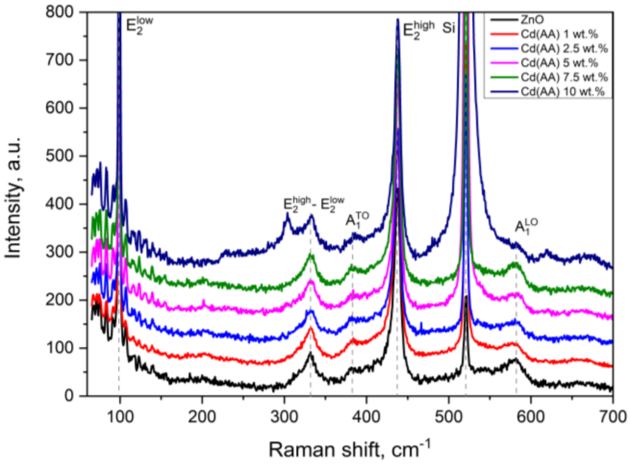

Fig. 6. Raman spectra of ZnO microstructures grown at various Cd(AA) concentrations.

The E_2^{high} frequency shift is substantial: from 437 cm^{-1} for pure ZnO to approximately 435.5 cm^{-1} for the doped samples. To take into consideration that E_2^{high} mode is associated with oxygen atoms, one can expect that the incorporation of Cd into ZnO lattice leads to the distortion of oxygen sublattice. As stated in [33] the E_2^{high} phonon in ZnO can exhibit a large variation of the frequency when either the isotopic masses of atoms constituting ZnO are changed or the homogeneously distributed impurities are present. Narrowing of both E_2^{low} and E_2^{high} until 5 wt.% and their latter broadening indicates that at Cd(AA) 5 wt.% the ZnO microstructures have the best crystallinity, and the following increase of Cd(AA) dopant leads to an increase of disorder in the crystal structure.

The shift of E_2^{high} mode indicates the presence of biaxial tensile stress in the plane of the substrate. To quantitatively evaluate the influence of stress on optical phonons, the frequency shift of the E_2^{high} mode ($\Delta\omega$) was analyzed as a function of lateral strain ε_{xx} [34] as follows,

$$\Delta\omega = 2\left(a - b\frac{C_{13}}{C_{33}}\right)\varepsilon_{xx} = m\varepsilon_{xx}\,, \qquad (5)$$

where $\Delta\omega = \omega - \omega_0$, $\omega_0 = 437.0$ cm^{-1} is the E_2^{high} phonon frequency of unstrained ZnO bulk crystal, $a = -690.8$ cm^{-1} and $b = -940$ cm^{-1} are phonon deformation-potential parameters, C_{13} = 105.1 GPa and C_{33} = 210.9 GPa are elastic constants of ZnO single crystal [35], and $m = -443$ cm^{-1} is the phenomenological coefficient. The obtained results for lateral strain ε_{xx} are also shown in Fig. 7.

3.3. Photoluminescence

The photoluminescence (PL) spectrum shown in Fig. 8 for all samples consists of four principal peaks at ultraviolet (NBE), blue (BB), yellow (YB), and infrared (IR) ranges. Despite a low Cd content in the grown samples, it is remarkable that the PL spectrum displays pronounced changes in PL intensity with increasing Cd(AA) amount. One can see that the near-band edge (NBE) peak in the spectrum of pure ZnO is observed at 3.27 eV, and shifts insignificantly to 3.26 eV in the spectra of the doped samples (1 to 5 wt.% of Cd(AA)). With further increase of Cd(AA) concentration (7.5…10 wt.%), the peak is smeared and its position shifts to 3.12 eV with a simultaneous decrease in the intensity. This shift can indicate a decrease in the band gap or the appearance of a number of energy levels in the forbidden band below the conduction band [36]. The bandgap energy $E_g(x)$ of the ternary alloy $Zn_{1-x}Cd_xO$ is determined by the following equation: $E_g(x) = 3.28(1 - x) + 2.3x - 3.04x(1 - x)$. Thus, the shift PL band to 3.12 eV can occur at 3 at.% of Cd. In our case, we did not observe such a significant Cd concentration in the EDX spectra. So, the appearance the new NBE2 peak at 3.12 eV is, apparently, due to the deterioration of crystal quality. This peak can be related to optical transitions via singly ionized oxygen vacancy [37, 38], transitions of free electrons to the level of zinc vacancy [39] or transition electron from Zn_i level to valence band.

Deep-level emissions (DLE) in ZnO are associated with defects in the crystal lattice, namely vacancies and interstitial defects. These defects include the surface states, zinc interstitials (Zn_i) and oxygen vacancies (V_O), which act as donors, and zinc vacancies (V_{Zn}) and oxygen interstitials (O_i), which act as acceptors [40].

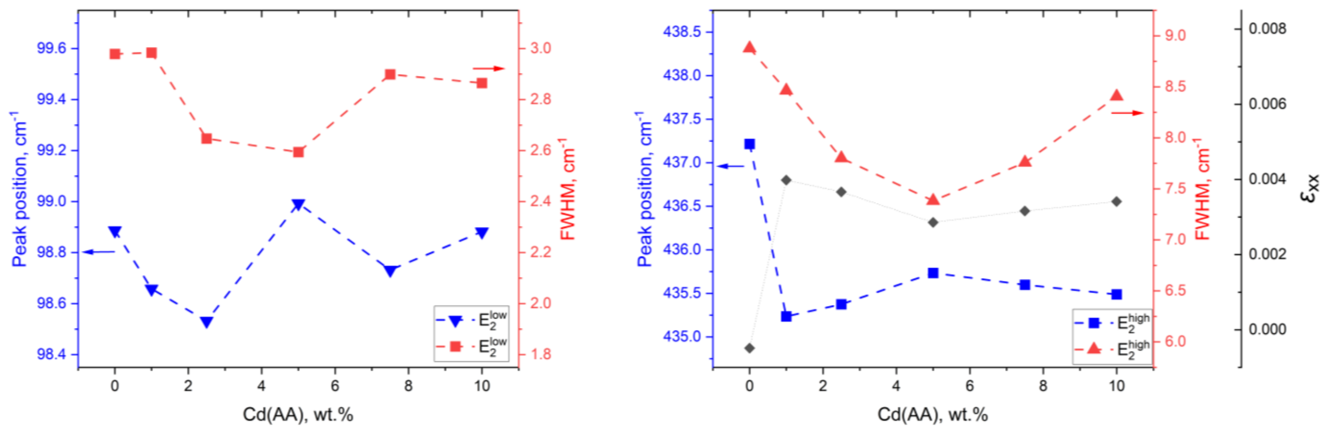

Fig. 7. Peak position shift and FWHM of E_2^{low} and E_2^{high} modes at various Cd(AA) concentrations.

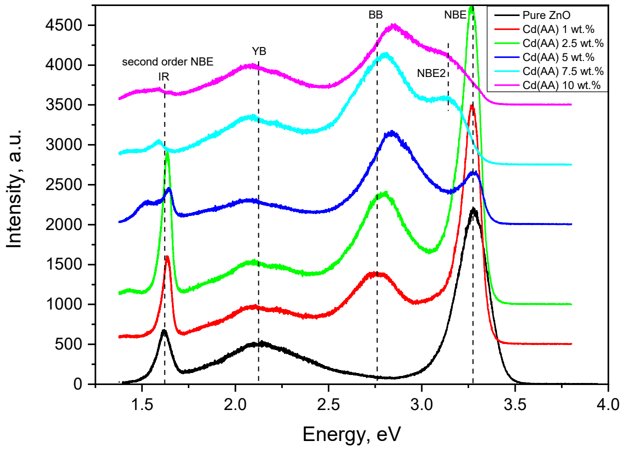

Fig. 8. PL spectra of grown zinc oxide microstructures at various Cd(AA) content.

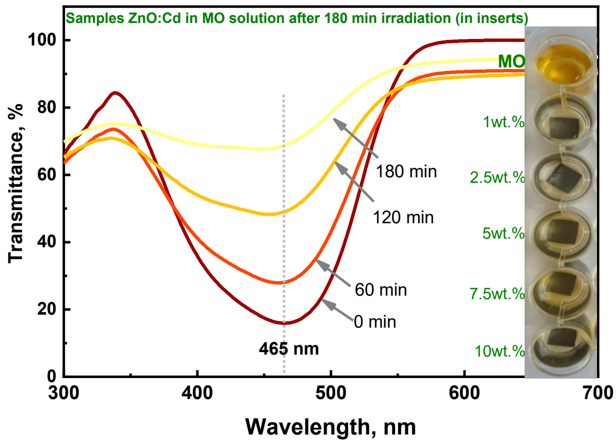

Fig. 10. Typical UV-VIS spectra of MO dye photodegradation in the presence of ZnO:Cd (2.5 wt.%) photocatalyst.

Emissions in the blue range (2.76…2.86 eV) are primarily linked to transitions involving Zn interstitials or Zn vacancies. Theoretically, Zn interstitials are positioned at 0.22 eV below the conduction band, and the V_{Zn} level is close to 0.3 eV above the valence band, enabling transitions from Zn_i to the valence band or to V_{Zn}, which can produce blue emission peaked at 2.8 eV [35]. The calculations in [26] suggest that Cd substitution at Zn sites reduces the formation energy of Zn vacancies. It is worth noting that the blue emissions are present only in the doped samples spectra. This indicates that Cd ions promote to formation Zn_i or V_{Zn} defects enhancing BB emission band. YB emission can occur from transitions free electrons from ZnO conduction band to O_i levels and the orange/red emission from transition electrons from shallow donor level of Zn_i to acceptor level of O_i. Finally, the emission peak in the near-infrared region (IR peak at 1.58…1.64 eV) reflects the second-order NBE emission. We have calculated the integral intensity for each bands and figured out their contribution to PL. The calculations were done in Origin program by using Lorentz function for each peak in non-linear curve fitting algorithm. The results are shown in Fig. 9.

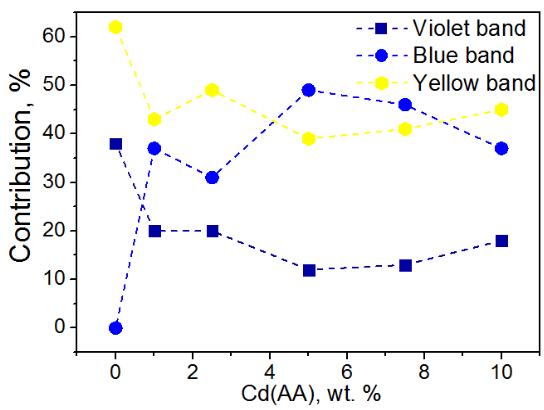

Fig. 9. Contribution to PL spectra of main violet, blue and yellow bands for ZnO microstructures at different Cd(AA) content.

The contribution of BB firstly increases to 50% at 5% of Cd(AA) then it decrease to 37 %. At the same time the behavior YB and NBE band looks the same. Thus, Cd impurity in initial acetylacetonate powder mixture stimulates formation of Zn_i or V_{Zn} defects in ZnO microstructures prepared by MOCVD at atmospheric pressure. The contribution of these defects in PL spectrum is significant 30–50%.

3.4. Photocatalytic study

The photocatalytic properties of ZnO and Cd-doped ZnO samples were investigated using Methyl Orange (MO) as a model pollutant. Methyl orange is one of the most widely used dyes in the textile industry and, at the same time, is very harmful to humans and animals [42]. The transmittance of the MO solution was monitored within the wavelength range 300…800 nm. This model dye has two absorption peaks in distilled water at 270 and 465 nm, respectively. The decrease of the peak at 465 nm was chosen to monitor the effect of MO degradation (Fig. 10) [43].

Fig. 11a shows the results of photodegradation of MO by pure ZnO and cadmium-doped ZnO photocatalysts after irradiation for 180 min. One can see that all Cd-doped samples of ZnO exhibit improved photocatalytic performance compared to pure ZnO. The highest efficiency of MO photodegradation was observed in ZnO:Cd (1 wt.%), ZnO:Cd (2.5 wt.%), and ZnO:Cd (10 wt.%). The photodegradation efficiency of the MO dye facilitated by these samples was 71%, 76% and 75%, respectively, after 180 min irradiation (Fig. 11b). At the same time, the photodegradation efficiency for undoped ZnO did not exceed 23%.

The kinetic rate constants (k) of MO degradation for all samples were calculated using Eq. (5) and shown in Fig. 12. The degradation rate constant k is determined from the $\ln(C_0/C_t)$ slope *vs* irradiation time (t) plot. The calculation results suggest that the photo-degradation of MO dye follows pseudo-first-order kinetics in the presence of Cd-doped ZnO photocatalysts. ZnO:Cd microstructures with lower concentrations of Cd(AA) (1 and 2.5 wt.%)

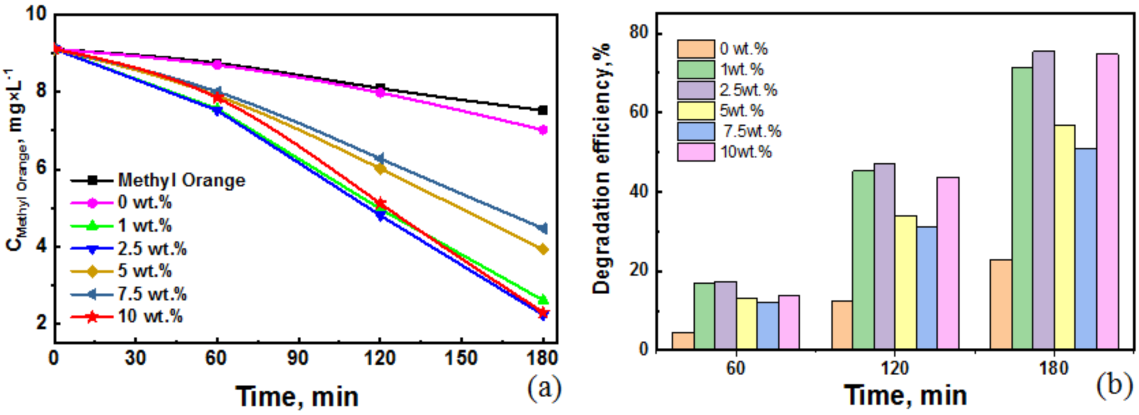

Fig. 11. Photodegradation rate of Methyl Orange dye in the presence of ZnO photocatalysts doped with Cd(AA) (0…10 wt.%) under Hg lamp irradiation (a), degradation efficiency of ZnO:Cd (0…10 wt.%) photocatalysts (b).

exhibited a higher reaction rate than samples with higher content of cadmium (5 and 7.5 wt.%). However, the sample with the highest Cd concentration (10 wt.%) also exhibits a high reaction rate. In this case, the influence of the surface morphology of the microstructures on the photocatalytic properties should not be neglected. Returning to the SEM results presented in Table 1, it is evident that the grain sizes in the samples with 2.5 and 10% of cadmium impurity are similar. In contrast, the samples with 5 and 7.5% cadmium impurity are characterized by a larger grain size and, accordingly, exhibit lower photocatalytic activity.

Based on our photoluminescence results, we can state that photodegradation is very efficient for samples with a 20% contribution of NBE emission into the PL spectrum and 30–40% of the blue band. The samples with intense blue emission demonstrate middle results. Clear ZnO microcrystals, due to intense UV emission, demonstrate the worst result. An increase in photo-catalytic activity for Cd-doped ZnO microcrystals can be explained by the appearance in the surface region of some surface states and intrinsic defects like V_{Zn}, photoexcita-tion of which allows the photogenerated electron-hole pair to overcome the solid-liquid barrier more easily, preventing their recombination through intrinsic defects, and facilitating various chemical reactions on the surface of the semiconductor catalyst.

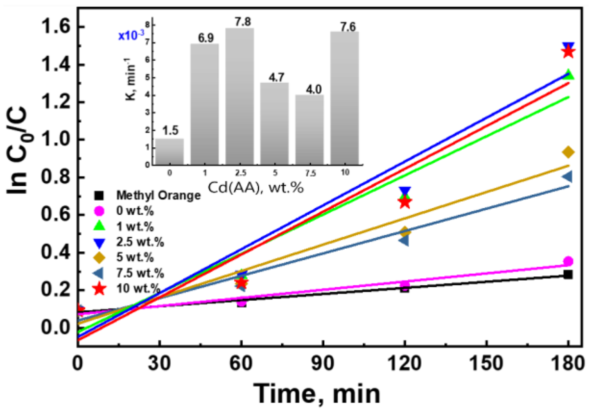

Fig. 12. Photodegradation kinetics in coordinates ln(C_0/C) *vs* time (t).

Furthermore, the enhanced photodegradation efficiency of Cd-doped ZnO nano-sheets, observed in the paper [44], was attributed to the increase in the defects and reduction in the bandgap of ZnO nanoparticles. The existence of Zn_i and V_{Zn} defects in the surface region of ZnO microstructures changes the Fermi level and promotes charge transfer.

4. Conclusions

This work investigated the effect of Cd dopant concentration on the properties of zinc oxide microstructures grown on silicon substrates by APMOCVD. The results of the X-ray diffraction analysis confirmed the formation of a crystalline phase of zinc oxide of the wurtzite type. The broadening of both E_2^{low} and E_2^{high} in Raman spectra at more than 5 wt.% of Cd(AA) indicates an increase of disorder in the crystal structure. Although Cd content in EDX analysis was not detected, photoluminescence and photocatalysis of ZnO microstructures grown with different Cd(AA) content demonstrate significant differences in PL. The decrease in intensity of NBE emission and its shift to lower energy were observed; the appearance of a blue band at 2.8 eV caused by Zn interstitials was also observed for Cd-doped ZnO microstructures compared to undoped ones. The photodegradation efficiency of the MO dye with undoped ZnO microstructures was only 23%. The maximum photocatalytic efficiency, above 70% after 180 min of irradiation, was observed in ZnO samples grown with 1, 2.5, and 10 wt.% Cd. The increase in photocatalytic activity of Cd-doped ZnO microcrystals can be explained by the existence of Zn_i and V_{Zn} defects in surface region of ZnO microstructures. These defects change Fermi level facilitating charge transfer. Thus, Cd-doped ZnO microstructures deposited on Si substrates are promising photocatalytic materials for effective photodegradation of toxic compounds in the environment.

Acknowledgements

This work was supported by the research grant of the National Academy of Sciences of Ukraine (№ 0125U000604).

References

1. Lemlikchi S., Abdelli-Messaci S., Lafane S. *et al*. Study of structural and optical properties of ZnO films grown by pulsed laser deposition. *Appl. Surf. Sci*. 2010. **256**. P. 5650–5655. https://doi.org/10.1016/j.apsusc.2010.03.026.
2. Kumar P., Kaushal S., Kumar S. *et al*. Recent advancements in pure and doped zinc oxide nanostructures for UV photodetectors application. *Phys. B: Condens. Matter*. 2025. **707**. P. 417177. https://doi.org/10.1016/j.physb.2025.417177.
3. Rahman F., Zinc oxide light-emitting diodes: a review. *Opt. Eng.* 2019. **58**. P. 010901. https://doi.org/10.1117/1.OE.58.1.010901.
4. Luo J. *et al*. Progress in perovskite solar cells based on ZnO nanostructures. *Solar Energy*. 2018. **163**. P. 289–306. https://doi.org/10.1016/j.solener.2018.01.035.
5. Golovynskyi S. *et al*. High transparent and conductive undoped ZnO thin films deposited by reactive ion-beam sputtering. *Vacuum*. 2018. **153**. P. 204–210. https://doi.org/10.1016/j.vacuum.2018.04.019.
6. Ievtushenko A. *et al*. Behavior of Al impurity in ZnO films: Influence of Al-level doping on structure, X-ray photoelectron spectroscopy and transport properties. *phys. status solidi (a)*. 2023. **220**. P. 2200523. https://doi.org/10.1002/pssa.202200523.
7. Baibara O., Radchenko M., Karpyna V., Ievtushenko A. A review of the some aspects for the development of ZnO based photocatalysts for a variety of applications. *Phys. Chem. Solid State*. 2021. **22**. P. 585–594. https://doi.org/10.15330/pcss.22.3.585-594.
8. Sun Y., Zhang W., Li Q. *et al*. Preparations and applications of zinc oxide based photocatalytic materials. *Adv. Sens. Energy Mater*. 2023. **2**. P. 100069. https://doi.org/10.1016/j.asems.2023.100069.
9. Mahmoud W.E., Al-Sanoosi A.M. Synthesis, characterization and photoluminescence of ZnO:Cd rosette-like nanostructures using solution process. *Superlattices Microstruct*. 2012. **51**. P. 506–511. https://doi.org/10.1016/j.spmi.2012.01.014.
10. Shtepliuk I. *et al*. Effects of Ar/O_2 gas ratio on the properties of the $Zn_{0.9}Cd_{0.1}O$ films prepared by DC reactive magnetron sputtering. *Acta Phys. Pol. A*. 2011. **120** (6-A), P. A-61–A-65. https://doi.org/10.12693/APhysPolA.120.A-61.
11. Mosquera E., del Pozo I., Morel M. Structure and redshift of optical band gap in CdO-ZnO nanocomposite synthesized by the sol-gel method. *J. Solid State Chem*. 2013. **203**. P. 265. https://doi.org/10.1016/j.jssc.2013.08.025.
12. Kasumov A., Korotkov K., Karavaeva V. *et al*. Photocatalysis with the use of ZnO nanostructures as a method for the purification of aquatic environments from dyes. *J. Water Chem. Technol*. 2021. **43**. P. 281–288. https://doi.org/10.3103/S1063455X21040044.
13. Altun B., Ajjaq A., Çağırtekin A.O. *et al*. Influence of isovalent Cd doping concentration and temperature on electric and dielectric properties of ZnO films. *Ceram. Int*. 2021. **47**. P. 27251–27266. https://doi.org/10.1016/j.ceramint.2021.06.147.
14. Ozugurlu E. Cd-doped ZnO nanoparticles: An experimental and first-principles DFT studies. *J. Alloys Compd*. 2021. **861**. P. 158620. https://doi.org/10.1016/j.jallcom.2021.158620.
15. Myroniuk D., Lashkarev G., Shtepliuk I. *et al*. Effect of high energy electron irradiation on structure and optical properties of ZnO films. *Acta Phys. Pol. A*. 2013. **124**, No 5. P. 891–894. https://doi.org/10.12693/APhysPolA.124.891.
16. Myroniuk D., Shtepliuk I., Lashkarev G. *et al*. Swift Xe ion irradiation effect on structure and vibrational properties of undoped and Cd-doped ZnO films. *phys. status solidi (c)*. 2014. **11**. P. 1435–1438. https://doi.org/10.1002/pssc.201300641.
17. Myroniuk D., Lashkarev G., Shtepliuk I. *et al*. Swift Xe^{26+} ion irradiation effect on luminescent properties of undoped and Cd-doped ZnO films. *Acta Phys. Pol. A*. 2014. **126**, No 5. P. 1199–1202. https://doi.org/10.12693/APhysPolA.126.1199.
18. Caglar Y. *et al*. Morphological, optical and electrical properties of CdZnO films prepared by sol–gel method. *J. Phys. D: Appl. Phys*. 2009. **42**. P. 065421. http://doi.org/10.1088/0022-3727/42/6/065421.
19. Vijayalakshmi S., Venkataraj S., Jayavel R. Characterization of cadmium doped zinc oxide (Cd : ZnO) thin films prepared by spray pyrolysis method. *J. Phys. D: Appl. Phys*. 2008. **41**. P. 245403. http://doi.org/10.1088/0022-3727/41/24/245403.
20. Acharya A.D., Moghe S., Panda R. *et al*. Effect of Cd dopant on electrical and optical properties of ZnO thin films prepared by spray pyrolysis route. *Thin Solid Films*. 2012. **525**. P. 49–55. https://doi.org/10.1016/j.tsf.2012.10.100.
21. Kuprenaite S., Murauskas T., Abrutis A. *et al*. Properties of In-, Ga-, and Al-doped ZnO films grown by aerosol-assisted MOCVD: Influence of deposition temperature, doping level and annealing. *Surf. Coat. Techn*. 2015. **271**. P. 156–164. https://doi.org/10.1016/j.surfcoat.2014.12.052.
22. Lupan O., Pauporté T., Chow L. *et al*. Comparative study of the ZnO and $Zn_{1-x}Cd_xO$ nanorod emitters hydrothermally synthesized and electrodeposited on *p*-GaN. *Appl. Surf. Sci*. 2012. **259**. P. 399–405. https://doi.org/10.1016/j.apsusc.2012.07.058.
23. Tortosa M., Mollar M., Mari B. Synthesis of ZnCdO thin films by electrodeposition. *J. Cryst. Growth*. 2007. **304**. P. 97–102. https://doi.org/10.1016/j.jcrysgro.2007.02.010.
24. Ievtushenko A., Tkach V., Strelchuk V. *et al*. Solar explosive evaporation growth of ZnO nanostructures. *Appl. Sci*. 2017. **7**. P. 383. https://doi.org/10.3390/app7040383.
25. Fouzri A., Boukadhaba M.A., Touré A. *et al*. Structural, morphological and optical properties of Cd doped ZnO film grown on a- and r-plane sapphire substrate by MOCVD. *Appl. Surf. Sci*. 2014. **311**. P. 648–658. https://doi.org/10.1016/j.apsusc.2014.05.131.
26. Debbichi M. *et al*. Room temperature ferromagnetism in Cd-doped ZnO thin films through defect engineering. *J. Alloys Compd*. 2014. **598**. P. 120–125. https://doi.org/10.1016/j.jallcom.2014.01.247.

27. Qaradawi S.A., Salman S.R. Photocatalytic degradation of methyl orange as a model compound. *J. Photochem. Photobiol. A: Chem*. 2002. **148**. P. 161–168. https://doi.org/10.1016/S1010-6030(02)00086-2.
28. Ahmad M., Ahmed E., Zhang Y. *et al*. Preparation of highly efficient Al-doped ZnO photocatalyst by combustion synthesis. *Curr. Appl. Phys*. 2013. **13**. P. 697–704. https://doi.org/10.1016/j.cap.2012.11.008.
29. Yamamoto K., Tsuboi T., Ohashi T. *et al*. Structural and optical properties of Zn(Mg,Cd)O alloy films grown by remote-plasma-enhanced MOCVD. *J. Cryst. Growth*. 2010. **312**. P. 1703–1708. https://doi.org/10.1016/j.jcrysgro.2010.02.029.
30. Patterson A.L. The Scherrer formula for X-ray particle size determination. *Phys. Rev*. 1939. **56**. P. 978–982. https://doi.org/10.1103/PhysRev.56.978.
31. Williamson B., Smallman R.C. Dislocation densities in some annealed and cold-worked metals from measurements on the X-ray Debye–Scherrer spectrum. *Phil. Mag*. 1956. **1**. P. 34. https://doi.org/10.1080/14786435608238074.
32. Xing Y.J., Xi Z.H., Xue Z.Q. *et al*. Optical properties of the ZnO nanotubes synthesized *via* vapor phase growth. *Appl. Phys. Lett*. 2003. **83**. P. 1689. https://doi.org/10.1063/1.1605808.
33. Alim K.A., Fonoberov V.A., Shamsa M., Balandin A.A. Micro-Raman investigation of optical phonons in ZnO nanocrystals, *J. Appl. Phys*. 2005. **97**. P. 124313. https://doi.org/10.1063/1.1944222.
34. Gruber Th., Prinz G.M., Kirchner C. *et al*. Influences of biaxial strains on the vibrational and exciton energies in ZnO. *J. Appl. Phys*. 2004. **96**. P. 289–293. https://doi.org/10.1063/1.1755433.
35. Liu W.-R., Lin B.H., Yang S. *et al*. The influence of dislocations on optical and electrical properties of epitaxial ZnO on Si (111) using a γ-Al_2O_3 buffer layer. *CrystEngComm*. 2012. **14**. P. 1665–1671. https://doi.org/10.1039/C2CE06218F.
36. Shtepliuk I.I., Lashkarev G.V., Khomyak V.V. *et al.* Influence of growth conditions on structural and optical properties of $Zn_{0.9}Cd_{0.1}O$ films. *Ukr. J. Phys.* 2012. **57**. P. 653–660. http://nbuv.gov.ua/UJRN/Ukjourph_2012_57_6_13.
37. Xu P.S., Sun Y.M., Shi C.S. *et al.* The electronic structure and spectral properties of ZnO and its defects. *Nucl. Instrum. Methods Phys. Res.* 2003. **199**. P. 286–290. https://doi.org/10.1016/S0168-583X(02)01425-8.
38. Mosquera E., Pozo I., Morel M. Structure and red shift of optical band gap in CdO–ZnO nanocomposite synthesized by the sol-gel method. *J. Solid State Chem*. 2013. **206**. P. 265–271. https://doi.org/10.1016/j.jssc.2013.08.025.
39. Kayaci F., Vempati S., Donmez I. *et al.* Role of zinc interstitials and oxygen vacancies of ZnO in photocatalysis: a bottom-up approach to control defect density. *Nanoscale*. 2014. **6**. P. 10224–10234. https://doi.org/10.1039/c4nr01887g.
40. Ievtushenko A., Karpyna V., Kolomys O. *et al.* Substrate bias influence on the properties of ZnO:Al and ZnO:Al,N films deposited by magnetron sputtering. *SPQEO*. 2024. **27**. P. 418–426. https://doi.org/10.15407/spqeo27.04.418.
41. Hsu C.-H., Chen L.-C., Zhang X. Effect of the Cu source on optical properties of CuZnO films deposited by ultrasonic spraying. *Materials*. 2014. **7**. P. 1261–1270. https://doi.org/10.3390/ma7021261.
42. Senthil Kumar M., Arunagiri C. Efficient photocatalytic degradation of organic dyes using Fe-doped ZnO nanoparticles. *J. Mater. Sci.: Mater. Electron*. 2021. **32**. P. 17925–17935. https://doi.org/10.1007/s10854-021-06328-0.
43. Karpyna V., Myroniuk L., Myroniuk D. *et al.* Effect of cobalt doping on structural, optical, and photocatalytic properties of ZnO nanostructures. *Catal. Lett*. 2024. **154**. P. 2503–2512. https://doi.org/10.1007/s10562-023-04493-x.
44. Kumar R., Umar A., Kumar R. *et al.* Low-temperature synthesis of cadmium-doped zinc oxide nano-sheets for enhanced sensing and environmental remediation applications. *J. Alloys Compd*. 2021. **863**. P. 158649. https://doi.org/10.1016/j.jallcom.2021.158649.

Authors' contributions

Karpyna V.A.: analyzing the data of experiments, writing and editing the original draft.
Lemish A.Ye.: analyzing the data of experiments, writing the original draft.
Myroniuk L.A.: writing and editing the original draft, analyzing the data of photocatalytic measurements.
Myroniuk D.V.: sample preparation, editing.
Olifan O.I.: performed XRD measurements.
Danylenko I.M.: performed RS, PL measurements.
Bilorusets V.V.: performed SEM, EDX measurements.
Starik S.P.: validation of SEM, EDX experimental data.
Strelchuk V.V.: validation of RS, PL experimental data.
Ievtushenko A.I.: key ideas, conceptualization, investigation, writing and editing the original draft, supervision.

Authors and CV

Vitalii A. Karpyna, Ph.D. in Physics and Mathematics, Senior Researcher at the Department of Physics and Technology of Photoelectronic and Magnetoactive Materials, Frantsevich Institute for Problems of Materials Science. Author of 164 publications. The main research activity covers the growth of thin films and nanostructures, investigation of structure, and optical and electrical properties of oxide semiconductors. E-mail: v.karpyna@ipms.kyiv.ua, https://orcid.org/0000-0002-1834-3672

Anatolii Y. Lemish, Bachelor of Micro- and Nano-System Technology, Technician of the I category at the Frantsevich Institute for Problems of Materials Science. Author of 3 publications. The main research activity covers the investigation of morphology, structure, photoluminescence and photocatalytic properties of ZnO:Cd nanostructures. https://orcid.org/0009-0001-9807-1186

Liliia A. Myroniuk, Ph.D. in Chemistry, Senior Researcher at the Department of Physics and Technology of Photoelectronic and Magnetoactive Materials, Frantsevich Institute for Problems of Materials Science. Author of 70 publications. The main research activity covers the growth of nanostructures by using the MOCVD method, investigation of morphology, structure and photocatalytic properties of oxide materials.
E-mail: l.myroniuk@ipms.kyiv.ua,
https://orcid.org/0000-0002-3113-1316

Denys V. Myroniuk, Ph.D. in Physics and Mathematics, Academic Secretary at the Frantsevich Institute for Problems of Materials Science. Author of 113 publications. The main research activity covers the growth of nanostructures by using APMOCVD method, investigation of structure, vibrational and optical properties of wide bandgap semiconductors.
E-mail:d.myroniuk@ipms.kyiv.ua,
https://orcid.org/0000-0002-1576-3671

Ihor M. Danylenko, Ph.D. in Natural sciences, Researcher at the Laboratory of Raman-luminescence and infrared Fourier spectroscopy at the V. Lashkaryov Institute of Semiconductor Physics. The main research activity covers Raman, PL and FTIR spectroscopy of semiconductor nanostructures, optical, phonon and electrical properties of semiconductors. E-mail: igor.tesV@gmail.com,
https://orcid.org/0000-0002-8740-204X

Olena I. Olifan, Researcher, Department of Physical Materials Science of Refractory Compounds at the Frantsevich Institute for Problems of Materials Science. Author of 150 publications. The main research activity is scanning and X-ray structural analysis of film samples, nanostructures and conductive undoped films obtained on various substrates. E-mail: o.olifan@ipms.kyiv.ua,
https://orcid.org/0000-0001-8007-607X

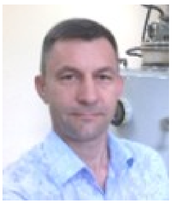

Viktor V. Bilorusets, Junior researcher of the Laboratory "Nanostructural and crystallophysical researches" at the V. Bakul Institute for Superhard Materials. The area of scientific interest includes the vacuum manufacture of coatings and the diagnostic of physics properties for materials.
E-mail: vbel71@ukr.net

Sergii P. Starik, Ph.D. in Materials Science. Head of the Laboratory "Nanostructural and crystallophysical researches" at the V. Bakul Institute for Superhard Materials. Authored over 100 publications and 7 patents. His research interests include diagnostic of physics properties of materials.
E-mail: starik@ism.kiev.ua,
https://orcid.org/0000-0003-1991-3275

Viktor V. Strelchuk, Doctor of Sciences, Professor, Leading Researcher at the Laboratory of submicron optical spectroscopy, V. Lashkaryov Institute of Semiconductor Physics. Authored over 300 publications, 10 patents, 6 textbooks. His scientific interests include optical spectroscopy of low-dimension structures, technology, physics and applications of semiconductors and their nanostructures, confocal Raman spectroscopy, FTIR.
E-mail: viktor.strelchuk@ccu-semicond.net,
https://orcid.org/0000-0002-6894-1742

Arsenii I. Ievtushenko, Ph.D. in Physics and Mathematics, Head of Department of Physics and Technology of Photoelectronic and Magnetoactive Materials at the Frantsevych Institute for Problems of Materials Science. Authored of over 280 publications. His research interests include solid-state physics, functional materials, and physical and chemical properties of oxide semiconductors.
E-mail: a.ievtushenko@ipms.kyiv.ua
https://orcid.org/0000-0002-8965-6772

Структура, оптичні та фотокаталітичні властивості легованих Cd мікроструктур ZnO, вирощених методом MOCVD за атмосферного тиску

В.А. Карпина, А.Є. Леміш, Л.А. Миронюк, Д.В. Миронюк, О.І. Оліфан, І.М. Даниленко, В.В. Білорусець, С.П. Старик, В.В. Стрельчук, А.І. Євтушенко

Анотація. Робота присвячена дослідженню впливу концентрації домішки кадмію на властивості мікроструктур оксиду цинку, вирощених на кремнієвих підкладках методом металоорганічного хімічного осадження з газової фази за атмосферного тиску. Рентгенограми підтверджують формування кристалічної фази оксиду цинку типу вюрцит. Спектри фотолюмінесценції мікроструктур ZnO складаються з декількох смуг, включаючи фіолетову (3,24 еВ), синю (2,8 еВ) і жовту (2,1 еВ). Синя смуга спостерігається тільки для мікроструктур ZnO, легованих Cd, і абсолютно відсутня для нелегованих мікроструктур ZnO. Мікроструктури ZnO, вирощені з 1, 2,5 і 10 мас.% Cd в суміші прекурсорів, продемонстрували найкращу фотокаталітичну ефективність (понад 70% деградації барвника метилового оранжевого протягом 180 хв). Вища константа швидкості реакції спостерігається для мікроструктур ZnO, легованих Cd, для яких внесок синьої смуги в загальний спектр ФЛ лежить у межах 30–40%, а внесок фіолетової смуги становить близько 20%. Одержані результати демонструють, що леговані Cd мікроструктури ZnO проявляють значну фотокаталітичну активність і можуть бути використані для розробки ефективних фотокаталізаторів.

Ключові слова: оксид цинку, кадмій, мікроструктури, MOCVD, фотокаталіз, фотолюмінесценція.